MRI SEGMENTATION USING MULTIFRACTAL ANALYSIS AND MRF MODELS

Su Ruan
CReSTIC, Dept GEII, IUT de Troyes, 10026 Troyes Cedex, France

Jonathan Bailleul
GREYC, ENSICAEN, 6 Bd. Maréchal Juin, 14050 Caen Cedex, France

Keywords: Multifractal analysis, Markov Random Field, image segmentation, Magnetic Resonance Imaging.

Abstract: In this paper, we demonstrate the interest of the multifractal analysis for removing the ambiguities due to the intensity overlap, and we propose a brain tissue segmentation method from Magnetic Resonance Imaging (MRI) images, which is based on Markov Random Field (MRF) models. The brain tissue segmentation consists in separating the encephalon into the three main brain tissues: grey matter, white matter and cerebrospinal fluid (CSF). The classical MRF model uses the intensity and the neighbourhood information, which is not robust enough to solve problems, such as partial volume effects. Therefore, we propose to use the multifractal analysis, which can provide information on the intensity variations of brain tissues. This knowledge is modelled and then incorporated into a MRF model. This technique has been successfully applied to real MRI images. The contribution of the multifractal analysis is proved by comparison with a classical MRF segmentation using simulated data.

1 INTRODUCTION

Image segmentation is a classical problem in computer vision and of paramount importance to medical imaging. Proper tissue classification enables: a) quantitative volumetric analysis on various brain structures; b) morphological analysis to assess intracranial deformation caused by brain tumours; c) visualisation for surgical planning and guidance.

In this paper, we deal with tissue segmentation of Magnetic Resonance Imaging (MRI) brain images. Numerous semi-automatic and automatic segmentation techniques have already been developed to replace manual segmentation which is a labour-intensive, subjective and thereby non reproducible procedure. Actually, the main techniques are based on: texture analysis (Schad,1993), histogram threshold determination (Suzuki, 1991), cluster analysis (Simmons, 1994) and fuzzy cluster analysis (Pham, 1999), a priori information about anatomy (Joliot, 1993), or MRF segmentation (Held, 1997)(Choi, 1997). Although there exists many image classification algorithms, the methods usually suffer from the fact that in practice there is a significant overlap in intensity values between tissue types, owing to magnetic field inhomogeneity, susceptibility artefacts and partial volume effects (one pixel mixed of two or more than two classes). Our idea, about this issue, is to describe the brain tissue using the relative intensity variations, rather than using only absolute intensity values. The multifractal analysis is adopted here to this objective. It was first introduced in the context of turbulence, and then studied as a mathematical tool as well as in many applications such as image processing (Sarkar,1995) (Levy-Véhel, 1996) (Grazzini, 2005). Due to the presence of noise in MRI images, it is important to take into account contextual information. This can be done a priori using MRF models which are appropriate to specify spatial dependencies by a priori label field distribution (Geman, 1984) (Choi,1997).

In this paper, we demonstrate the interest of the multifractal analysis to remove the ambiguities due to the intensity overlap and propose a tissue segmentation method based on Markov Random

Ruan S. and Bailleul J. (2007).
MRI SEGMENTATION USING MULTIFRACTAL ANALYSIS AND MRF MODELS.
In *Proceedings of the Second International Conference on Computer Vision Theory and Applications*, pages 101-106
DOI: 10.5220/0002046901010106

Field (MRF) models. The brain segmentation consists in separating the encephalon into the three main brain tissues: grey matter, white matter and CSF. The classical MRF model uses the intensity and the neighbourhood information, but it is not robust enough to solve the problems such as partial volume effects. Therefore, we propose to supplement the multifractal analysis to the classical MRF model, which can provide the information about intensity variations of the brain tissues.

2 MULTIFRACTAL ANALYSIS OF IMAGES

It is well known that the geometrical complexity of a "fractal" set may be described, in a global way, by giving its dimension. In order to describe the local singular behaviour of measures or signals, the multifractal analysis is proposed to give either geometrical or probabilistic information about the distribution of points having the same singularity (Levy-Véhel, 1996, 2000). The value of Hölder exponent α is usually used to obtain a local information about the pointwise regularity. The so-called "multifractal spectrum" $f(\alpha)$ gives the geometrical or probabilistic information. Some spectra, such as Hausdorff spectrum f_h and large deviation spectrum f_g, have been defined and studied (Levy-Véhel,1998). The multifractal analysis of images usually consists in computing values of Hölder exponentα and its multifractal spectrum, then classifying each point according both to the value of Hölder exponent α and to the corresponding spectrum $f(\alpha)$. In this paper, we are only interested in the local information provided by the Hölder exponent α.

2.1 The Hölder Exponent α

Let μ be a Borel probability measure laid upon a compact set P. For each point x in P, the Hölder exponent α can be defined as follows (Levy-Véhel, 1996)(Canus 1996) (more rigorous and complete definitions are given in (Brown, 1992) (Levy-Véhel,1998)):

$$\alpha(x) = \lim_{\delta \to 0} \frac{\log \mu(B_\delta(x))}{\log \delta} \qquad (1)$$

where $B_\delta(x)$ is an open-ball of diameter σ centred on the point x. It reflects the local behaviour of the measure μ around x. In image analysis, the points in the equation (1) are naturally associated to the pixels of the image, the open-balls to windows in 2D and balls in 3D centred on each pixel, the measures to functions of grey level intensities. In our case, the measure μ is defined as the sum of the grey level intensities of pixels within a neighbourhood $V(\delta)$ defined by a ball of diameters σ. The Hölder exponent α can be assessed as the slope of $\log[\mu(V(\delta))]$ versus $\log \delta$. δ changes linearly from 1 to the maximum value with unity step. If the maximum diameter of the neighbourhood is chosen small, α reacts to localize singularities. If the maximum diameter is large, α reacts to more widespread singularities. Thanks to the choice of the measure function $\mu(V(\delta))$, we can obtain the following local information via the Hölder exponent: let us note α0 the Hölder exponent within a intensity uniform (homogeneous) region. If the value of α for the current pixel is higher than $\alpha 0$, it is surely within a intensity concave region (valley), while in the inverse case, the current voxel is in a intensity convex region (hill). The illustration of the different values of α is shown in Figure 1. In fact, $\mu(V(\delta))$ in a concave region increases more rapidly in function of $V(\delta)$ than that in a convex region. The value α0 lies between them.

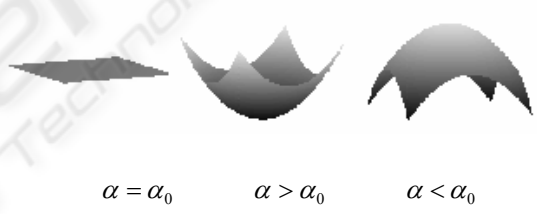

Figure 1: Illustration of α for different spatial variations of intensity.

2.2 MRI Images

The local image information provided by α is very helpful in the situation of low contrast, since it can discriminate the three situations described above. As known, the cortex of the brain has many circumvolutions. Thus, it leads to intensity variations in image, which can be easily described by the multifractal analysis. In MRI images, the sulcus can be considered as a valley in term of intensity, and the CSF is generally at the bottom of the valley. On the contrary, the gyrus can be considered as a hill, and the white matter, surrounded by the grey matter, is at the top of the hill. The problems of the partial volume effects and of the low contrast are essentially present in these two types of regions. Most of the homogeneous regions can be found within the white matter (in the

center of the brain) and a few others within the grey matter. The Figure 2 shows one axial MRI slice in which examples of the three types of region are pointed out.

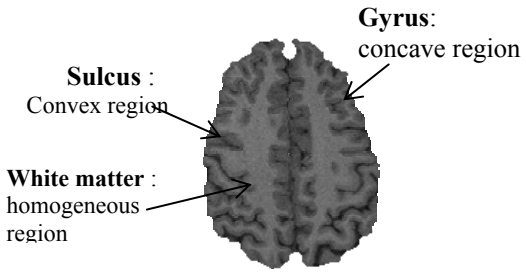

Figure 2: Three regions in MRI data: convex, concave and homogeneous region.

The difficulties of the segmentation are mainly founded in the regions of the gyri and sulci due to the partial volume effects. The a priori knowledge about these two regions described by the Hölder exponent α can help us to cope with this problem. The histogram of α obtained from a T1-wheighted MRI data set (256×256×124 pixels, with a resolution of 0.9375×0.9375×1.2mm³) is shown in Figure 3. Its form is always concave for the MRI data, because of the brain morphology. In fact, the area of the homogeneous region, usually in white matter, is larger than that of the others regions (concave and convex regions). Therefore, α_0 describing an homogeneous region, can be easily found by detecting the peak of the histogram. Since we are just interested in three types of region (concave, homogeneous and convex), and do not pay attention to the degree of concavity or convexity, we can define a function $f(\alpha)$ as follows to obtain the three types of region :

$$f(\alpha) = \begin{cases} 1 & if \quad \alpha(x) < \alpha_0 \\ 0 & if \quad \alpha(x) = \alpha_0 \\ -1 & if \quad \alpha(x) > \alpha_0 \end{cases} \qquad (2)$$

Figure 4 shows one α slice (the original image is shown in Figure 2) and the three types of region obtained using (2) : concave, convex and homogeneous regions. The measure region is a cube of 3×3×3 pixels. The value of $\alpha 0$, found from the peak of the histogram of α is 2.29. Comparing to the original image, it can be observed that the homogeneous regions correspond mainly to the white matter, and the values of α correctly reflect the hills and valleys in the image.

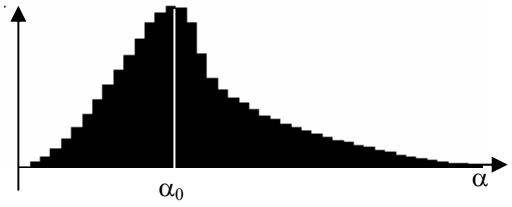

Figure 3: Histogram of α calculated from a 3D MRI volume. The measure region is 3x3x3 voxels.

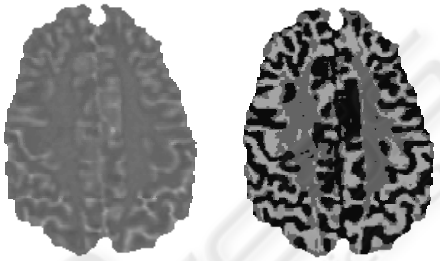

Figure 4: One slice of α image (left) and the three types of region (right): convex region in deep grey colour, concave region in white colour and homogeneous in light grey colour.

3 MARKOVIAN SEGMENTATION

We propose to incorporate a priori information about multifractal characterisation into the MRF model. Let us consider three random fields*: Y={Ys, s∈S}* represents the field of observations located on a lattice S of N sites s, *X={Xs, s∈S}* the label field and *A={αs, s∈S}* the multifractal field. Each *Ys* takes its value in Λ_{obs}*={0...,255},* each *Xs* in {1=CSF, 2=gray matter, 3=white matter} and each *As* in *{-1,0,1}* (see equation (2)). We use the Bayes rule to write:

$$P(x_s / y_s, \alpha_s) = \frac{P(y_s, \alpha_s / x_s) P(x_s)}{P(y_s, \alpha_s)} \qquad (3)$$

Since the two fields *Ys* and *As* are independent, (3) becomes:

$$P(x_s / y_s, \alpha_s) = \frac{P(y_s / x_s) P(\alpha_s / x_s) P(x_s)}{P(y_s, \alpha_s)} \qquad (4)$$

We look for the x_s that maximises the left-hand side of (4). Since $P(y_s, \alpha_s)$ does not depend on the x_s, this is equivalent to write:

$$\hat{x}_s = \arg\max_{x_s} P(y_s / x_s) P(\alpha_s / x_s) P(x_s) \qquad (5)$$

In accordance with the Hammersley and Clifford theorem (Geman, 1984), $P(x_s)$ is defined by a Gibbs distribution,

$$P(x_s) \equiv \frac{1}{Z}\exp(-U_2(x_s)) \quad (6)$$

where U2 stands for the energy function and Z is a normalising constant.

Denoting $P(y_s/x_s)=\frac{1}{Z'}\exp(-U_1(y_s/x_s))$ and

$P(\alpha_s / x_s) = \frac{1}{Z''}\exp(-U_3(\alpha_s / x_s))$, Eq.(6) can be defined in terms of an energy function that has to be minimised:

$$\hat{x}_s = \arg\min_{x_x}\{U_1(y_s / x_s) + U_2(x_s) + U_3(\alpha_s / x_s)\} \quad (7)$$

- Let us consider the terms U1. In MRI data, the distribution of the grey levels of each tissue has a gaussian form, and there is no correlation between them. The data energy term is thus expressed as :

$$U_1(y_s / x_s) = \frac{(y_s - m_{x_s})^2}{2\sigma_{x_s}^2} + \ln(\sqrt{2\pi}\sigma_{x_s}) \quad (8)$$

- Let's consider now $U_2(x_s)$, the energy term corresponding to the a priori model. We adopt a 3D system of second-order neighbourhood C, consisting of the 18 nearest neighbours. Using standard isotropic Potts model, one obtains :

$$U_2(x_s) = -\beta\sum_{s,t\in C}(1-\delta(x_s, x_t)) \quad (9)$$

where β is a weight coefficient, and is the Kronecker delta function. U_2 is minimum for a homogeneous region.

- The energy term $U3(\alpha_s/ x_s)$ is defined in order to advantage the choice of the CSF label or white matter label for a site whether it is in a convex region or a concave region respectively. Since only two types of region are interesting in our case, $U3(\alpha_s/ x_s)$ can be defined according to $f(\alpha)$. It becomes :

$$U_3(\alpha_s / x_s) = f(\alpha_s)\begin{cases}\kappa_{convex} & \text{if } x_s = 1\\ -\kappa_{concave} & \text{if } x_s = 3\\ 0 & \text{otherwise}\end{cases} \quad (10)$$

where $\kappa_{concave}$ and κ_{convex} are constant (>0).

If one pixel has a grey level near the middle of the means of the CSF and the gray matter or the middle of the means of the grey matter and the white matter, its U_1 is not dominant. The classification of this pixel depends mainly on the U_2 and U_3 terms. Therefore, the a priori information brought by U_3 is very useful in this case.

We use the deterministic relaxation algorithm ICM (Besag, 1974) to minimise the global energy function U. For the initialisation, we exploit a maximum likelihood segmentation depending only on U_1.

4 RESULTS

In order to show the improvement of the segmentation by addition of the multifractal term U3, simulated MRI data were used, which are available on the site BrainWeb (Collins,1998). This three-dimensional phantom is made up of ten volumetric data sets that define the spatial distribution of different tissues (e.g. grey matter, white matter, CSF, etc), where the voxel intensity is proportional to the fraction of tissue within the voxel. A threshold value equal to 50% can be used to obtain the voxels belonging to the corresponding tissue, which is considered as the gold standard. Each volume data consists of 181×217×181 voxels, whose size is 1×1×1mm3. The simulated MRI volume with a noise level of 7% is used for our study. It was firstly segmented by the software developed in our laboratory (Moretti, 2000) to obtain the encephalon in which there are only the three brain tissues (Figure 5).

The segmentation results are evaluated by measuring the sum, denoted ξ_{total}, of the false positive ratio ξ_{fp} and the false negative ratio ξ_{fn}. ξ_{fp} is defined as the number of misclassified voxels divided by the number of good voxels taken from the gold standard (N). The false negative ratio ξ_{fn} is defined as the number of lost good voxels divided by N.

In order to obtain the initial values of the means and the variances used in $U_1(y_s/x_s)$ to carry out the initialisation of the segmentation, we used the Davidon-Fletcher-Powell method described in (Press, 1992) to fit the intensity histogram of the encephalon data set by a sum of three gaussian functions. Since the phantom is relatively realistic, studies on the choice of the parameters used in the models were carried out. The parameters β and κ can be chosen in the ranges $\beta\in[0.1, 0.5]$ and $\kappa\in[0.5,1.5]$ which provide acceptable ξ_{total}. According to our experience, the algorithm ICM is not very sensitive to the value βbut rather to the initialisation of the

segmentation. To reduce this dependence on the initialisation, the means and variances are re-estimated at each iteration. A comparison of the results obtained by the classical Markovian segmentation and the proposed segmentation method is performed and shown in Table 1 (β =0.2, κ_{convex} = $\kappa_{concave}$ =1.1). We can observe that the total error ξ_{total} on each tissue is reduced using the function U_3 in addition. As discussed above, the a priori information modelled by U_3 can ameliorate the results in the case of low contrast. These cases are usually apparent in the boundaries of tissues or in gyri and sulci, which represent a small percentage of total volume data. That is why the improvement is about 2%. The errors for the CSF segmentation seem to be more than those for the others. That is because the number of CSF voxel is much lower than those of the other tissues, thus it easily results a high relative error ratio.

Real MRI data were also used to evaluate visually the results. The corresponding result of the image shown in Figure 2 is illustrated in Figure 6. Compared to the classical Markovian segmentation, the segmentation integrating the multifractal information favours the sulci and gyri if the contrast, due to the partial volume effects, is low in these regions. Two small windows are located in Figure 6 to show the amelioration in critical regions. The discontinuities of the white matter and sulci obtained by the classical MRF segmentation are significantly repaired by the proposed method. To illustrate more clearly this issue, volume-rendered images of the white matter are used (Figure 7). As known, the white matter of the human is a continuously connected structure, thus the volume-rendered image using the proposed method depicts more accurately the white matter.

5 CONCLUSION

We have presented a MRF segmentation method incorporating the a priori multifractal information model, aiming to segment MRI brain tissues. The Hölder exponent α permits to describe locally the intensity variations, therefore helping to remove the ambiguities due to the low contrast and the partial volume effects. Three types of region: concave, convex and homogeneous region are used in our model. The results obtained on the digital phantom and the real MRI data show quantitatively and qualitatively improvement of the brain segmentation.

Although the empirical values, chosen for the model parameters (β, κ_{convex} and $\kappa_{concave}$), give satisfying results, adapted values to different volume data will be more efficient and make the segmentation more accurate. The estimation of these hyperparameters is an important issue in the future work.

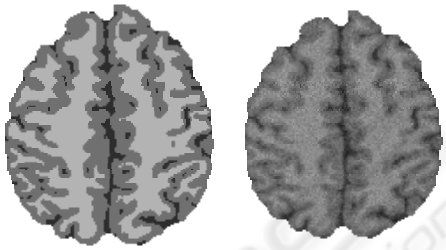

Figure 5: One slice of gold standard (left) and the corresponding slice of the simulated data with a level noise of 7% (right). The three tissues are colour-coded as follows: white matter =white colour, grey matter =grey colour, CSF =black.

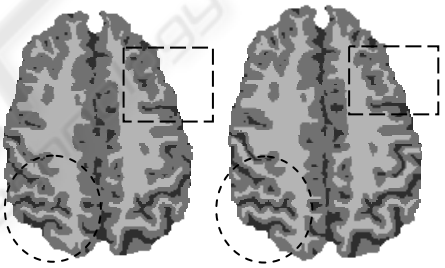

Figure 6: Comparison of results of the slice shown in Figure 2 with (right) and without (left) use of the multifractal analysis. Three tissues are obtained: white matter (white colour), grey matter (grey colour) and CSF (black). The improvements can be observed in the circle windows concerning the white matter and the rectangular windows concerning the CSF.

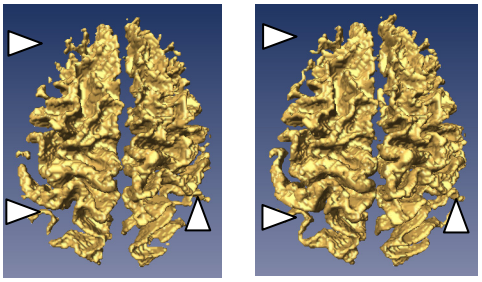

Figure 7: Volume-rendered images of the white matter obtained from the classical MRF segmentation (left) and the proposed segmentation method (right). Some discontinuities of structures (left) and improvements (right) are pointed out by arrows.

Table 1: Comparison of the results obtained by the classical MRF segmentation (Method 1) and by the proposed method (Method 2), using the false positive ratio ξ_{fp} and the false negative ratio ξ_{fn}.

Tissue	Method 1 (%)			Method 1 (%)		
	ξ_{fp}	ξ_{fn}	ξ_{total} %)	ξ_{fp}	ξ_{fn}	ξ_{total}
WM	3.12	8.50	11.62	3.88	5.87	9.7
GM	7.99	5.02	13.01	6.19	5.09	11.2
CSF	13.37	7.78	21.15	10.76	8.78	19.

REFERENCES

Besag, J., 1974. On the statistical analysis of dirty pictures. J.R. Statist. Soc. B-48, 259-302.

Brown, G., Michon, G. and Peyrière, J., 1992. On the Multifractal analysis of measures. J.Stat. Phys. 66, 775-790.

Canus, C., Lévy-Véhel, J., 1996. Change detection in sequences of images by multifractal analysis. Proc. of ICASSP'96, May 7-10, Atlanta.

Choi, S. M., Lee, J. E. and Kim, M. H., 1997. Volumetric object reconstruction using the 3D-MRF model-based segmentation, IEEE. Trans. Med. Imag.16, 887-892.

Collins, D.L. and al., 1998. Design and construction of a realistic digital brain phantom. IEEE. Trans. Med. Imag.,17, 463-468 (http: //www.bic.mni.mcgill.ca /brainweb).

Geman, S. and Geman, D., 1984. Stochastic relaxation, Gibbs distribution, and the Bayesian restoration of images. IEEE Trans. Pattern Analysis and Machine Intelligence 6, 721-741.

Grazzini, J., Turiel, A., Yahia, H., 2005. Presegmentation of high-resolution satellite images with a multifractal reconstruction scheme based on an entropy criterium. Proceeding of IEEE ICIP-2005, Volume: 1, On page(s): I- 649-52.

Held, K., Kops, E. R., Krause, B. J., Wells, W. M., Kikinis, R. and Müller-Gärtner, H. W., 1997. Markov Random Field segmentation of brain MR images, IEEE. Trans. on Med. Imag. 16, 878-892.

Joliot, M. and Mazoyer, B., 1993. Three-dimensional segmentation and interpolation of magnetic resonance brain images. IEEE Trans. Med. Imag.12, 269-277.

Levy-Véhel, J., 1996. Introduction to the multifractal analysis of images. In Fractal Encoding and analysis. Yuval Fisher Editor, Springer Verlag.

Levy-Véhel, J., Vojak, R., 1998. Multifractal analysis of choquet capacities: preliminary results. Adv.in Appl. Math. 20, 1-43.

Levy-Véhel, J., 2000. Signal enhancement based on Hölder regularity analysis. In IMA Volumes in Mathematics and its Applications, Volume 132, pp. 197-209.

Moretti, B., Fadili, J., Ruan, S., Bloyet, D. and Mazoyer, B., 2000. Phantom-based performance evaluation-application to brain segmentation from magnetic resonance images. Medical Image Analysis, Vol. 4, No. 4, pp. 303-316, June, 2000.